Journal of Power Sources 264 (2014) 140–146

Contents lists available at ScienceDirect

Journal of Power Sources

journal homepage: www.elsevier.com/locate/jpowsour

Short communication

Study of the deterioration mechanism of $LiCoO_2$/graphite cells in charge/discharge cycles using the discharge curve analysis

Kohei Honkura [a,*], Tatsuo Horiba [b]

[a] Hitachi Research Laboratory, Hitachi, Ltd., 7-1-1, Omika, Hitachi, Ibaraki 319-1292, Japan
[b] Department of Chemistry for Materials, Graduate School of Engineering, Mie-University, 1577 Kurimamachiya-cho, Tsu, Mie 514-8507, Japan

HIGHLIGHTS

- An advanced differential voltage analysis was applied to $LiCoO_2$/graphite cells.
- Initial cell capacities were controlled by the negative electrode.
- Positive electrode came to control the cell capacities after 500 cycles.
- The accuracy of the differential voltage analysis lowered after this switch.

ARTICLE INFO

Article history:
Received 27 December 2013
Received in revised form
27 March 2014
Accepted 7 April 2014
Available online 18 April 2014

Keywords:
Lithium ion batteries
Discharge curve analysis
Capacity fading
Differential voltage

ABSTRACT

The differential discharge curve analysis that separates the discharge curve of battery cells into those of the positive and negative electrodes is useful for investigating deterioration mechanisms. We applied it to $LiCoO_2$/graphite cells and investigated the capacity fading mechanisms during charge/discharge cycles. In the initial state, the discharge curves of the cells were reconstructed very well by the discharge curves of the positive and negative electrodes measured in advance. The discharge curve analysis revealed that the initial cell capacities were controlled by the negative electrodes. On the other hand, the capacity of the positive electrode decreased faster than that of the negative electrode during the course of the cycle test. With repeated charge/discharge cycles, the positive electrodes came to control the cell capacities. After that, deep charge/discharge cycles of the positive electrode accelerated the loss of capacity and the increase of the internal resistance. Furthermore, the rapid increase of the internal resistance lowered the accuracy of the discharge curve analysis. Although the discharge curve analysis was still applicable to the cells that were controlled by the positive electrodes, there were some discrepancies around the end-points of the discharge curves.

© 2014 Elsevier B.V. All rights reserved.

1. Introduction

Lithium-ion batteries are now being introduced into various applications which demand long battery lifetimes. This makes the clarification of the degradation mechanism of lithium-ion batteries much more important than before in order to guarantee their lifetimes. The conventional procedure of studying the degradation mechanism requires disassembling the degraded lithium-ion cells into the positive electrode, the negative electrode, the separators and the electrolytes. After that, the electrochemical properties of the half-cells are measured, or they are analyzed with various techniques such as XRD, XPS and TEM. Although this procedure supplies us with various sorts of information on the degradation, we cannot observe the deterioration continuously. There is also the concern that removing the elements from the degraded cells alters them from when they were in the degraded cells.

Non-destructive analyses do not have such problems, but they are not generally informative. The best way to assess the degradation of the positive electrode and the negative electrode separately is to analyze the charge/discharge curves of the lithium-ion cells [1–3]. Bloom et al. developed a non-destructive "differential voltage analysis" using the relationship between discharged capacity Q and differential voltage dV/dQ [1]. They focused on the peaks appearing in the Q vs dV/dQ curves of the cells that indicate transitions in the structure of the positive or negative active materials. Because every peak is attributable to a certain density of

* Corresponding author. Tel.: +81 294 52 5111; fax: +81 294 52 7636.
E-mail address: kohei.honkura.tt@hitachi.com (K. Honkura).

http://dx.doi.org/10.1016/j.jpowsour.2014.04.036
0378-7753/© 2014 Elsevier B.V. All rights reserved.

lithium in the positive or negative electrodes, the distances between the peaks help us to decide the capacity of both electrodes and the mutual "slippage" of the Q vs dV/dQ curves of the positive and negative electrodes.

Taking advantage of the preceding works, we have developed a mathematically-advanced differential voltage analysis technique with which we can precisely and visually separate the discharge curves of lithium-ion cells into those of the positive and negative electrodes [4]. In the process of separation, the usable masses of the positive and negative active materials and the "slippages" of the positive and negative electrodes are quantitatively evaluated. Furthermore, the irreversible lithium-ion loss consumed in SEI growth can be derived from the results of the discharge curve analysis. We applied this analysis to the results of calendar life test of cells including a manganese-based layered structure oxide for the positive electrode and hard carbon for the negative electrode [5]. With this cell, we observed moderate capacity fading and confirmed that the dominant deterioration mechanism was SEI growth.

In this paper, we applied our mathematically-advanced differential voltage analysis to $LiCoO_2$/graphite cells in order to confirm the applicability of this analysis to various cell chemistries. We investigated the degradation mechanisms in these cells and discovered that the loss of usable mass of the active material would be the dominant degradation mechanisms in these cells unlike to the cells used in our previous work in which the SEI growth was the constantly dominant degradation mechanism. We also discovered the switching of the dominant degradation mechanism changed the rate of degradation of the cells. Moreover, we discovered the case that the discharge curve analysis could not reproduce the experimental discharge curve of the cells measured even at C/50, which was never shown in our previous work.

2. Experimental

2.1. Charge/discharge-cycle life tests

We fabricated 1.1 Ah-class prismatic cells (48 mm × 33 mm × 5.0 mm) and measured their discharge curves during charge/discharge-cycle life tests. The positive electrode consisted of 97% (weight) $LiCoO_2$ active material, 2% carbon conductive material, and 1% PVDF binder. The negative electrode consisted of 98% graphite active material and 2% styrene-butadiene rubber binder with carboxymethyl cellulose. The positive electrode contained 7.97 g of active materials, while the negative contained 3.66 g. The positive and negative electrodes were formed on both sides of aluminum and copper foils by an ordinary slurry coating process. Both of the finished electrodes were wound together with separators and sealed into a prismatic can with an electrolyte of 1 mol L^{-1} lithium hexafluorophosphate in a mixture of organic carbonates.

After initial conditioning, the initial rate capabilities and thicknesses of the cells were measured. In the rate capability measurement, the cells were charged for 2 h at 1.1 A to 4.2 V in CC/CV mode, rested for 2 h, discharged to 2.5 V at 0.022, 0.22, 0.55, 1.1, 1.65, 2 or 3 A in CC mode, and rested for 2 h at 25 °C. The thicknesses of the cells were measured at the center of the side faces (48 mm × 33 mm) at room temperature with a micrometer. The cells were then subjected to a charge/discharge-cycle life test. The cells were charged for 2 h to 4.2 V at 1.1 A in CC/CV mode, rested for 0.5 h, discharged to 2.5 V at 1.1 A in CC mode and rested for 0.5 h at 25 °C in the charge/discharge cycle. Every 100 cycles, the rate capabilities and thicknesses of the cells were measured as mentioned above. A battery testing system, TOSCAT-3000, Toyo System Co., was used for the charge/discharge-cycle life tests.

2.2. Half-cell tests

We measured the discharge curves of the positive and negative electrodes in advance in order to use them to reproduce the discharge curves of the full cells. We used half cells consisting of a pristine 1.8 cm^2 positive or negative electrode (small pieces of electrodes with the same specifications as the test cells) as the working electrode, a separator, an electrolyte, and lithium foil as the counter and reference electrode. They were assembled in an argon glove box at room temperature. Then we charged and discharged them 15 times at 0.1 mA (less than a $C/50$ rate) between 3.0 and 4.3 V for the positive electrode and between 0.005 and 1.5 V for the negative electrode. The TOSCAT-3000 was used for the charge/discharge tests for the half-cells.

2.3. Discharge curve analysis

Fig. 1 illustrates the relationships among the discharge curves and related parameters. The cell capacity Q is represented by

$$Q = m_p q_p - \delta_p = m_n q_n - \delta_n, \tag{1}$$

where q_p and q_n are the specific discharge capacities of the active materials, m_p and m_n are the usable active material masses, and δ_p and δ_n are the marginal capacities. The differential voltage of the cells dV/dQ is expressed as

$$\frac{dV_{cell}(Q)}{dQ} = \frac{dV_p(Q)}{dQ} - \frac{dV_n(Q)}{dQ} = \frac{1}{m_p}\frac{dV_p(q_p)}{dq_p} - \frac{1}{m_n}\frac{dV_n(q_n)}{dq_n} \tag{2}$$

where $V_p(q_p)$ and $V_n(q_n)$ are the specific discharge curves. The differential discharge curves measured at 0.022 A were reproduced with appropriate m_p, m_n, δ_p and δ_n based on Eqs. (1) and (2).

The capacity corresponding to irreversible lithium-ion loss Li_{loss} was estimated from the analysis. The increasing rate dLi_{loss}/dt is expressed as

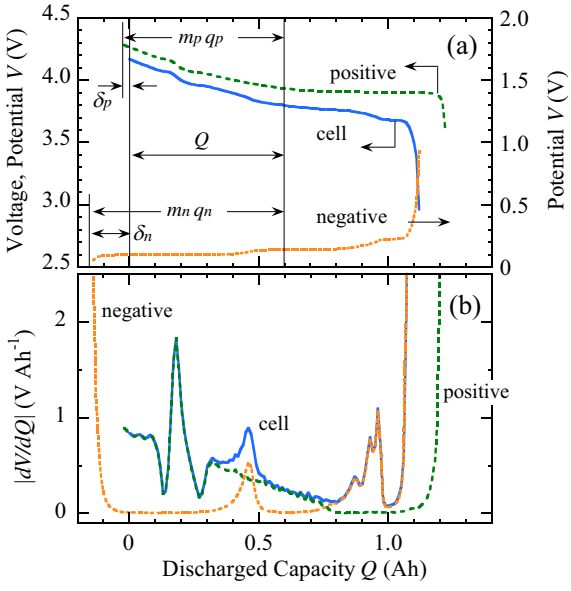

Fig. 1. Schematic view of the discharge curve analysis: the relationship among parameters and discharge curves.

$$\frac{\mathrm{dLi_{loss}}}{\mathrm{dt}} = m_\mathrm{n}\frac{\mathrm{d}q_\mathrm{n}}{\mathrm{d}t} - m_\mathrm{p}\frac{\mathrm{d}q_\mathrm{p}}{\mathrm{d}t} = \frac{\mathrm{d}(\delta_\mathrm{n}-\delta_\mathrm{p})}{\mathrm{d}t} - q_\mathrm{n}\frac{\mathrm{d}m_\mathrm{n}}{\mathrm{d}t} + q_\mathrm{p}\frac{\mathrm{d}m_\mathrm{p}}{\mathrm{d}t}. \tag{3}$$

The increments of $\mathrm{Li_{loss}}$ over 100 charge/discharge cycles from the starting time t_1 to the ending time t_2 were estimated by simplifying the integral of Eq. (3) as

$$\Delta\mathrm{Li_{loss}} \cong \delta_\mathrm{n}(t_2) - \delta_\mathrm{n}(t_1) - \delta_\mathrm{p}(t_2) + \delta_\mathrm{p}(t_1) - \langle q_\mathrm{n}\rangle[m_\mathrm{n}(t_2) - m_\mathrm{n}(t_1)] + \left\langle q_\mathrm{p}\right\rangle[m_\mathrm{p}(t_2) - m_\mathrm{p}(t_1)] \tag{4}$$

where $<q_\mathrm{p}>$ and $<q_\mathrm{n}>$ are the average specific capacities for each 100 cycles at which the usable mass of active materials were deemed to decrease. The details of the discharge curve analysis were described in our previous paper [5].

3. Results & discussion

3.1. Specific discharge curves of electrodes

Fig. 2 shows the discharge curves of the positive electrode: Fig. 2(a) shows the half-cell's experimental discharge curves; Fig. 2(b) shows the transformed discharge curves per unit mass of the positive active material. As shown in Fig. 2(a), the capacities and the shape of the discharge curves changed as the number of cycles increased. These experimental discharge curves $V(Q)$ and $\mathrm{d}V/\mathrm{d}Q(Q)$ are transformed into the discharge curves $V(q)$ and $\mathrm{d}V/\mathrm{d}q(q)$ by the following equation

$$q = \frac{Q}{m}, \quad \frac{\mathrm{d}V}{\mathrm{d}q} = m\frac{\mathrm{d}V}{\mathrm{d}Q} \tag{5}$$

where m is the usable mass of the active material that was used as a fitting parameter. The transformed discharge curves in Fig. 2(b) agreed below 0.14 Ah g^{-1}, while they disagreed above 0.14 Ah g^{-1}. This disagreement in the fully discharged state may suggest a cycle-by-cycle micro fluctuation of the reaction area in the positive electrode. The $\mathrm{Li}_x\mathrm{CoO}_2$ has a two-phase coexistence domain of the conductive and insulating phases for $0.75 \le x \le 0.94$ corresponding to the plateau near 3.9 V [6,7]. And $\mathrm{Li}_x\mathrm{CoO}_2$ turns to be insulating for $x > 0.94$ or below 3.9 V. When insulating parts form over the electric contact points between the active materials and the conductive materials, the active materials seem to become unusable even if they have some residual useful conductive parts. Thus, we thought that the transformed discharge curve with the maximum capacity was the closest to the specific discharge curve of the positive active materials. We used the transformed discharge curve of the first cycle as the specific discharge curve in the discharge curve analysis.

Fig. 3 shows the discharge curves of the negative electrode: Fig. 3(a) shows the half-cell's experimental discharge curves; Fig. 3(b) shows transformed discharge curves per unit mass of the negative active material. The transformations were based on Eq. (5) in a similar way to those of the positive electrodes. However, in the case of the negative electrodes, we fixed the fully discharged states in the transformed discharge curve to 0.372 Ah g^{-1} or $y = 0$ in $\mathrm{Li}_y\mathrm{C}_6$ because y does not reach 1 at the fully charged states when the graphite crystal structure has disorders [8]. The transformed discharge curves agreed well above 0.2 Ah g^{-1}. At the same time, the peaks around 0.18 Ah g^{-1} sharpened as the number of charge/discharge cycles increased. This change may suggest that the phase transition from the stage-1 to the stage-2 occurred more uniformly after many cycles than after a few cycles. The volume changes of the graphite during charge/discharge cycles may assist the uniform transition of the graphite by adjusting the positions of the particles and relaxing the stress between them, which prevents volume changes during phase transition. Thus, we used the transformed discharge curve at the 15th cycle as the specific discharge curve of the negative active material in the discharge curve analysis.

3.2. Charge/discharge cycle life

Fig. 4 shows the full discharge capacities of the cells, Q_full, which were measured in the rate capability measurements mentioned above, from 4.2 to 2.5 V at various currents I from 0.022 to 3.0 A every 100 cycles during the charge/discharge cycle test. The dashed lines are the regression lines of the relationship between I and Q_full. The capacities decreased as the cycle number increased, except for the capacities at 3.0 A before 100 cycles. There are two points to be noted: one is the constant decreases of Q_full at 0.022 A, and the other is the decreases of the slopes $\mathrm{d}Q_\mathrm{full}/\mathrm{d}I$ of the regression lines. The capacities at 0.022 A decreased rather monotonically as shown

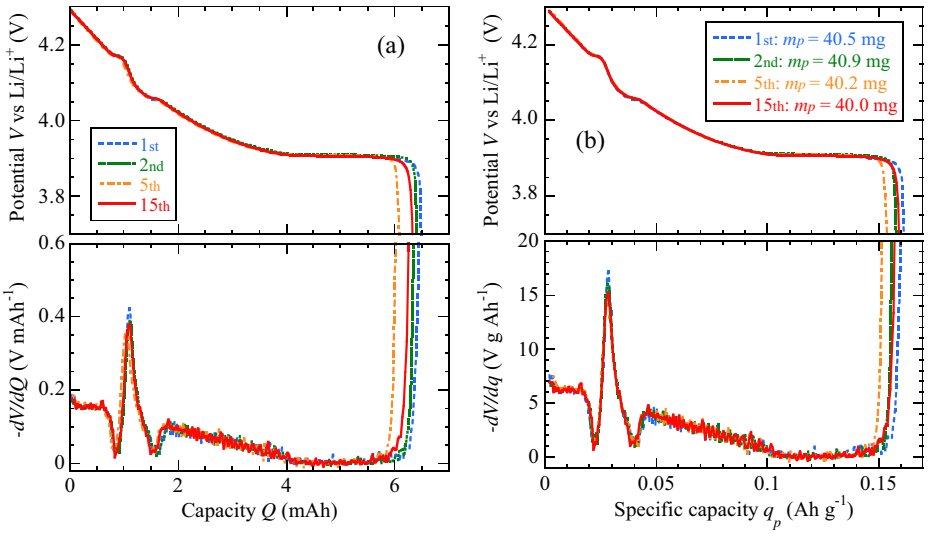

Fig. 2. The discharge curves of the positive electrode: (a) the experimental discharge curves and (b) the transformed discharge curves.

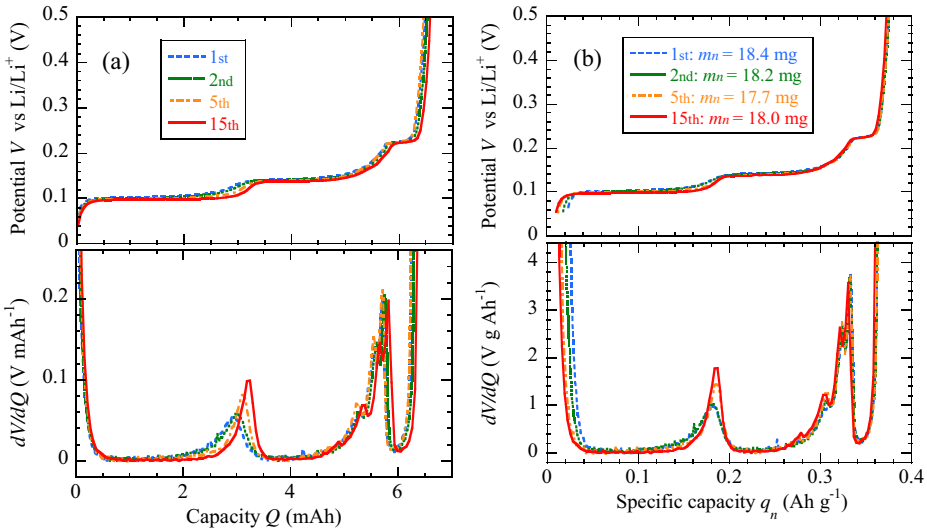

Fig. 3. The discharge curves of the negative electrode: (a) the experimental discharge curves and (b) the transformed discharge curves.

in Fig. 5. Meanwhile the slopes dQ_{full}/dI were almost the same up to 700 cycles, after which they decreased rapidly. The rapid decrease of dQ_{full}/dI indicates that the internal resistances of the cells increased more rapidly after 700 cycles than before.

Fig. 6 shows the direct-current internal resistances of the cells measured in the rate capability measurement. They were calculated by the slopes of the regression line between the discharge currents, 0.11, 0.22, and 0.55 A and the corresponding over-voltages at 1 s after start discharge. The resistances increased rather moderately before 500 cycles, then increased more rapidly. The change of the increasing rate of resistance happened 200 cycles earlier than the rapid decrease of dQ_{full}/dI shown in Fig. 5.

Fig. 7 shows the cell thicknesses measured every 100 cycles and the amount of increase during each 100-cycle segment. From 100 to 700 cycles, the thickness increment slightly decreased or rather stayed constant as the cycle number increased. However, the increment began to grow steeply after that. Fig. 4 also shows similar change after 700 cycles. That is to say, the gradients of the rate capability from 100 to 700 cycles are almost the same, however those after that increases steeply. In Fig. 6, the internal resistance increments after 700 cycles show much larger values than those before. The similarity shown by these results seems to suggest their common root cause.

Fig. 8 shows the results of the discharge curve analysis. The experimental discharge curves of the cells in Fig. 8(a)–(d) were measured at 0.022 A, while that in Fig. 8(e) was measured at 0.01 A. Fig. 8(a) shows the discharge curves just after initialization, Fig. 8(b) shows them after 400 cycles, Fig. 8(c) shows them after 600 cycles, and Fig. 8(d) and (e) shows them after 900 cycles. The discharge curves just after initialization and after 400 cycles were reproduced well through the whole area from the starting point to the ending point. On the other hand, the discharge curves after 600 and 900 cycles were not reproduced well in the whole area. Thus we limited the area to reproduce the discharge curves and extrapolated the curves to the whole area using the parameters for the limited area. The discharge curve of the cells after 600 cycles from 0 to 0.7 Ah was reproduced well. However, the extrapolated discharge curve above 0.7 Ah deviated from the experimental discharge curve. In addition, the calculated cell capacity for 0.79 Ah was smaller than the experimental cell capacity for 0.83 Ah. There was the same tendency in the results of the analysis for the discharge curves after 900 cycles. The discharge curve of the cells from 0 to 0.43 Ah was reproduced well, while the extrapolated discharge curve above 0.43 Ah deviated from the experimental curve. The calculated cell

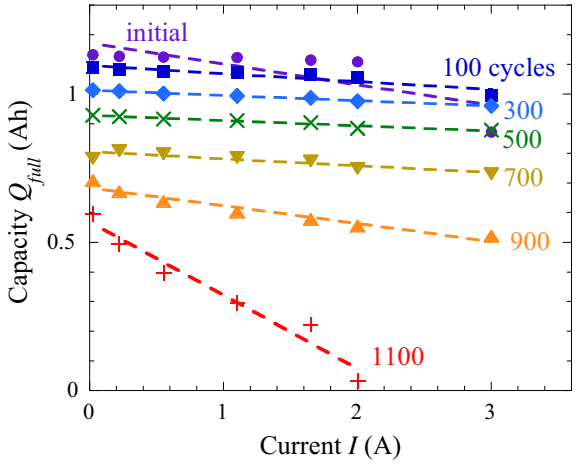

Fig. 4. The discharge capacity of the cells measured at various currents, from 0.022 to 3.0 A, during the charge–discharge cycle life test.

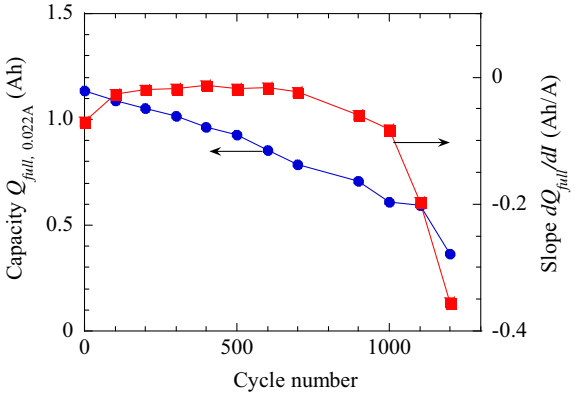

Fig. 5. The discharge capacities of the cells at 0.022 A and the slopes of the regression lines of the relationship between the discharge currents and the discharge capacities.

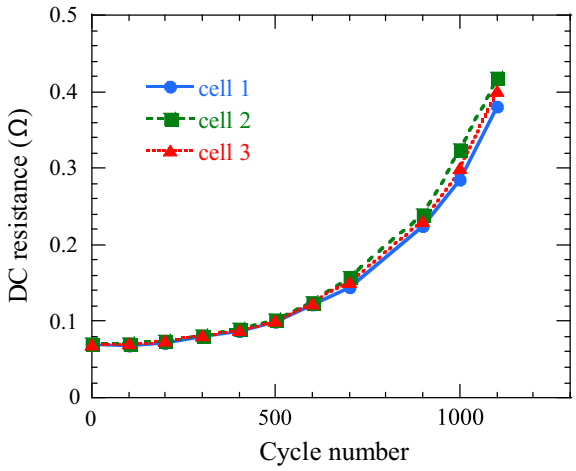

Fig. 6. The direct-current internal resistances of the cells measured in the rate capability measurement at 0.11, 0.22 and 0.55 A.

capacity for 0.51 Ah was smaller than the experimental one for 0.69 Ah. When the discharge current was reduced to 0.01 A, the agreement between the experimental and extrapolated discharge curves above 0.43 Ah slightly improved. It indicates that the influence of the internal resistance became significant above 0.43 Ah after 900 cycles or less. However, the discharge curves measured at 0.022 and 0.01 A were almost the same below 0.43 Ah, which implied that the influence of the internal resistance was not dominant below 0.43 Ah both at 0.022 and 0.01 A. Thus, the discharge curve analysis should be used only to interpret the first half of the discharge curve of the cells after 600 cycles. Some modification is necessary to apply the analysis to longer cycle life test results accompanying significant increment of internal resistance.

The cell voltage dropped at the same point as the abrupt rising of the negative electrode potential in Fig. 8(a) and (b), which revealed that the cell capacities were controlled by the negative electrode. On the other hand, the cell voltage dropped at the same point as the dropping of the positive electrode potential. This clear contrast implied that the positive electrode controlled the cell capacity after 600 cycles.

Fig. 9 shows changes of the full capacities of the positive and negative electrodes, the capacities of the cells Q_{full} measured at 0.022 A, and the capacities of the irreversible lithium-ion loss ΔLi_{loss} due to the side reactions. The full capacities of the positive

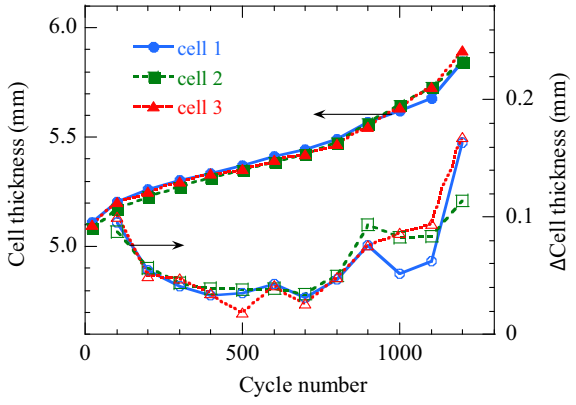

Fig. 7. The thicknesses of the prismatic cells measured every 100 cycles during the charge–discharge cycle test and the amount of increase (Δ cell thickness) during each 100-cycle segment.

and negative electrodes were calculated by multiplying the maximum specific capacities 0.162 Ah g^{-1} for m_p and 0.372 Ah g^{-1} for m_n. In Fig. 1, they correspond to the capacities between the left and right ends of the positive and negative discharge curves. The capacities of the irreversible lithium-ion loss ΔLi_{loss} were calculated based on Eq. (4) with $<q_p>$ and $<q_n>$ values which correspond to a cell voltage of 4.2 V. It does not directly appear in Fig. 1, but it is strongly related to the difference of marginal capacities, $\delta_n - \delta_p$, as shown in Eqs. (3) and (4). After 600 cycles, the discharge curve analysis was applicable only to the first half of the discharge curve of the cells. Thus the full capacities after 600 cycles were calculated from the analysis of the first half and shown in Fig. 9 in dotted lines to imply low accuracy. The correct ΔLi_{loss} were not calculated after 600 cycles either. However, rough estimation of ΔLi_{loss} after 600 cycles was possible because all δ_n, δ_p, $<q_p>$ for 4.2 V, and $<q_n>$ for 4.2 V were calculated from the first half of the discharge curve of the cells. The accuracy of the dotted lines should be verified by our future work along with the mechanism of the disagreement. These three capacities, $0.162m_p$, $0.372m_n$, and ΔLi_{loss}, represent the three presumably independent degradation mechanisms, the loss of sites for lithium ions in the positive and negative electrodes and the loss of lithium ions. The comparison of them in Fig. 9 shows that the losses of the negative electrode's capacity and the capacities of the irreversible lithium-ion loss were comparable in magnitude, while the loss of the positive electrode's capacity was larger than they. Moreover, we can see that the losses of the cell capacity do not agree with any of these three, which means that there is no single dominant degradation mechanism for the cell capacity. This deterioration behavior is quite different from the case of our previous work on the cell chemistry of manganese-based layered oxide/hard carbon [5]. The loss of the cell capacity was nearly equal to ΔLi_{loss} and the SEI growth was clearly dominant deterioration mechanism throughout the whole calendar life in our previous work.

3.3. Deterioration mechanism

The rate capability of the cells in Fig. 5 rapidly degraded after 700 cycles and the direct-current internal resistances in Fig. 6 rapidly increased after 500 cycles in the charge/discharge-cycle life test. Furthermore, the discharge curve analysis revealed that the cell capacities were controlled by the negative electrodes before 400 cycles, while they were controlled by the positive electrode after 600 cycles as shown in Fig. 8. In addition, the experimental discharge curves of the cells before 400 cycles were reproduced well in the whole area, while they were not well reproduced around the discharge endpoint after 600 cycles.

These results suggest which electrode controls the cell capacity is very important for the cell performance degradation and the accuracy of the discharge curve analysis. Fig. 10 shows the endpoint capacities of the discharge curves of the positive and negative electrodes and the cells. The positive and negative electrodes' endpoint capacities, $0.162m_p - \delta_p$ and $0.372m_n - \delta_n$, correspond to the capacities at the right ends of the positive and negative discharge curves in Fig. 1. The endpoint capacities of the cell are the capacities at 2.7 V on the discharge curves of the cells. The calculated endpoint capacities of the cells are almost equal to the smaller of the positive and negative endpoint capacities. The endpoint capacities after 600 cycles were shown in dotted lines because of the poor reproducibility of the discharge curves around endpoints as shown in Fig. 8(c)–(e). The controlling electrode for the cell capacities seemed to change from the negative electrode to the positive electrode after 500 cycles. After that, the calculated endpoint capacities of the cells deviated from the experimental ones. This change of the controlling electrode after 500 cycles coincided with the rapid increase of the internal resistances.

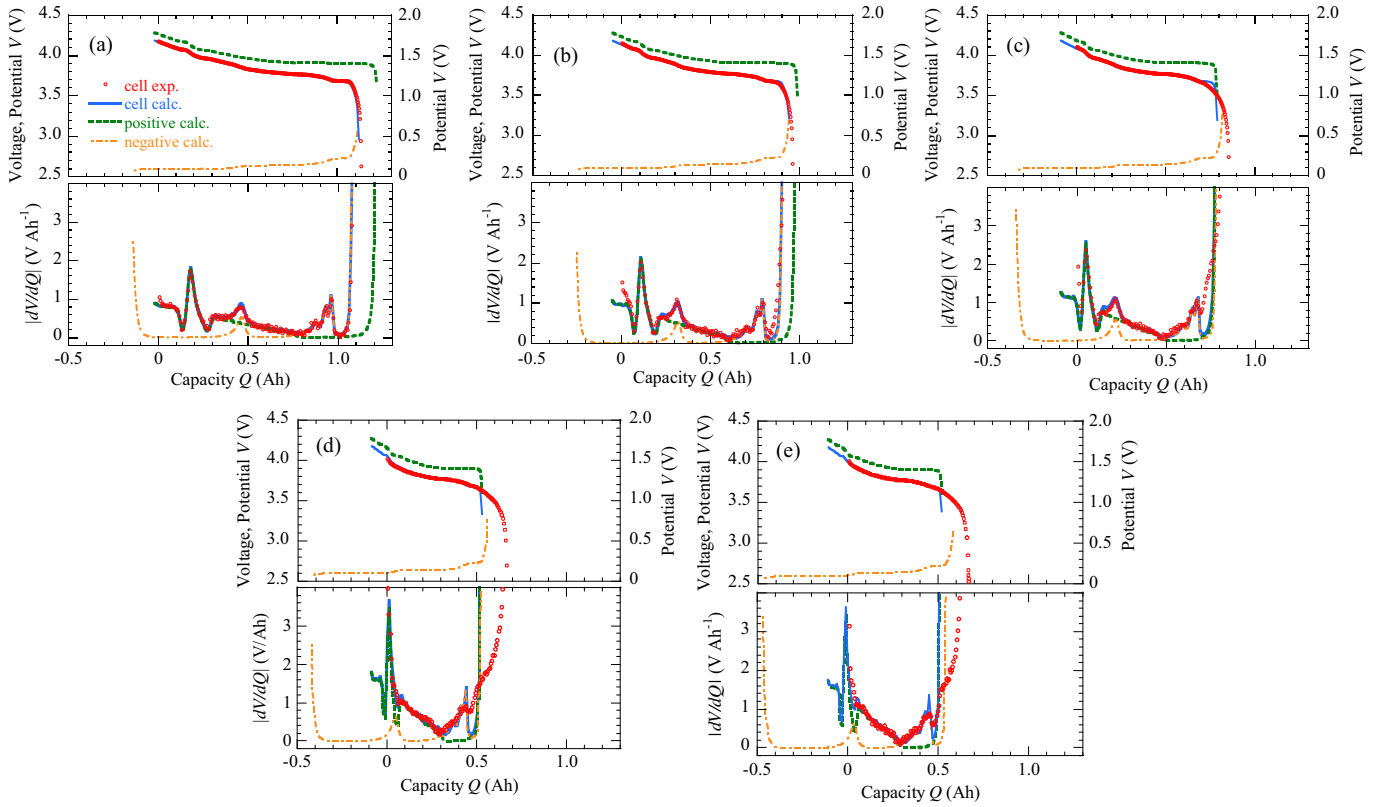

Fig. 8. The results of the analysis for the discharge curves of the cells measured (a) just after initialization, (b) after 400 cycles, (c) after 600 cycles, and (d) after 900 cycles at 0.022 A. The discharge curve of the cell for (e) was measured after 900 cycles at 0.01 A.

Based on these data and analysis, we supposed that the cells degraded in the cycle life tests as follows. The decrease of the capacity of the positive electrode was apparently larger than that of the negative electrode through the whole stage of the cycle test, as shown in Fig. 9. However, in the early stage of the charge/discharge-cycle life test, the endpoint capacities of the discharge curves of the positive electrode remained larger than those of the negative electrode as shown in Fig. 8(a) and (b). Thus, the capacity fading of the positive electrode did not appear in the capacity of the cells. The capacity fading of the cells in this stage was almost the same as the sum of that of the negative electrode and the irreversible lithium-ion loss as shown in Fig. 9. It is noted that the irreversible lithium-ion loss shifts the discharge curve of the negative electrode to the left in Fig. 1 and decreases the endpoint capacity of the discharge curve of the negative electrode as shown in Fig. 8(a) and (b). The degradation of the cell performance was rather moderate in this stage. However, the endpoint capacities of the discharge curves of the positive electrodes neared those of the negative electrodes, and they met after 500 cycles, as shown in Fig. 10. In addition, the positive active materials came to be fully discharged at the end of discharge of the cells. Thus the crystal structure of $LiCoO_2$ changed from the conductive/insulating coexistence phases to the single insulating phase [6], and the internal resistance in the positive electrode became much larger as shown

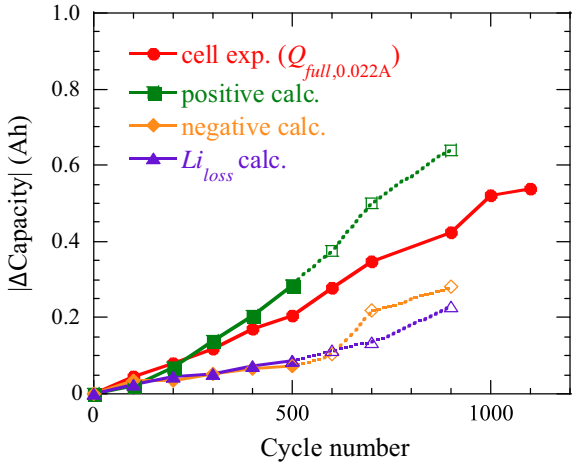

Fig. 9. Capacity change from the initial for the cell, the positive electrode, the negative electrode, and the irreversible lithium-ion loss.

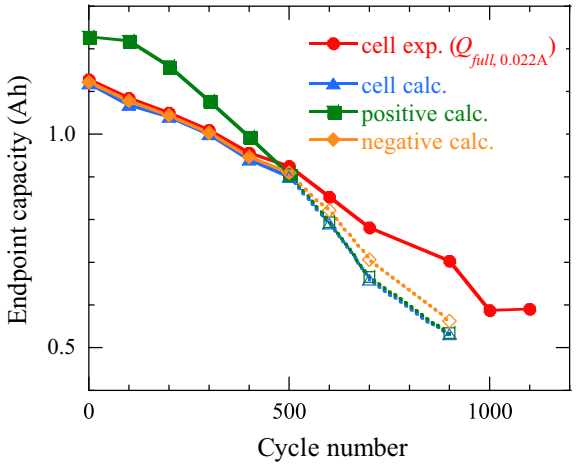

Fig. 10. The experimental endpoints of the discharge and the calculated curves of the cells, the positive electrode, and the negative electrode.

in Fig. 6, which gradually increased loads to the residual usable masses of the active materials during charge/discharge cycling. Consequently, the lowering of the rate capabilities was accelerated as shown in Fig. 5. The large internal resistance against intercalation/de-intercalation of lithium likely assists the gas-generating side reactions in the positive electrode [9] which might be responsible for the cell swelling shown in Fig. 7 and the decrease of the rate capability.

One problem remaining to be solved is the difference between the experimental and calculated discharge curve of the cells in the second half after 600 cycles. The differences were partially attributed to the increasing internal resistance as shown in Fig. 8(d) and (e). However, the excess capacities near the endpoints of discharge curve of the cells in Fig. 8(c)–(e) were not expected from the influence of the increasing internal resistance. The excess capacity must be caused by quantitative or qualitative changes in the positive active materials at least. We suppose that some active material particles were partially disconnected from the electron conductive network by the deformation of the electrode structure, and they contributed to the discharge capacity only when the current was very low and the potential difference between the surrounding particles was large. This speculation is not verified at present. Change of the cell design parameters such as the amount of conductive material or the capacity ratio of the negative to the positive electrodes, or change of discharge mode would help to explore the questions.

4. Conclusion

We applied our mathematically-advanced differential voltage analysis to the $LiCoO_2$/graphite cells and confirmed the applicability of the analysis to the cell chemistry as well as to the cell chemistry of the manganese-based layered structure oxide and hard carbon we used in a previous paper [5]. Using the analysis, we investigated the deterioration mechanism of the cells in a charge/discharge-cycle life test. The dominant degradation factor of the cells alternates from the capacity fading of the negative electrode and the irreversible lithium-ion loss to the capacity fading of the positive electrode. After the switch, the internal resistance of the cells increased rapidly because of forming the insulating phase of the positive active material. Moreover, after the switch, the discharge curves of the cells calculated using the analysis deviated from the experimental curves around their endpoints. This disagreement indicates the necessity for further improvement of the analysis and might suggest guidelines to refine it. The influence of increasing internal resistance and the resulting change of the specific discharge curves of the positive and negative electrodes should be taken into consideration in order to improve this analysis in further works.

References

[1] I. Bloom, A.N. Jansen, D.P. Abraham, K.L. Gering, J. Power Sources 139 (2005) 295–303.
[2] A.J. Smith, J.C. Burns, J.R. Dahn, Electrochem. Solid-State Lett. 14 (2011) A39–A41.
[3] Q. Zhang, R.E. White, J. Power Sources 179 (2008) 785–792.
[4] K. Honkura, H. Honbo, Y. Koishikawa, T. Horiba, ECS Trans. 13 (19) (2008) 61.
[5] K. Honkura, K. Takahashi, T. Horiba, J. Power Sources 196 (2011) 10141–10147.
[6] M. Ménétrier, I. Saadoune, S. Levasseur, C. Delmas, J. Mater. Chem. 9 (1999) 1135–1140.
[7] J.N. Reimers, J.R. Dahn, J. Electrochem. Soc. 139 (1992) 2091–2097.
[8] T. Zheng, J.R. Dahn, Phys. Rev. B 53 (1996) 3061–3071.
[9] D. Aurbach, B. Markovsky, A. Rodkin, E. Levi, Y.S. Cohen, H.-J. Kim, M. Schmidt, Electrochim. Acta 47 (2002) 4291–4306.